Experimental data: Electrolyte effects on hydrodynamics in an airlift bubble column

Manas M. Mandalahalli, Evert C. Wagner, Luis M. Portela*, Robert F. Mudde

Transport Phenomena group, Department of Chemical Engineering, Delft University of Technology, Delft, the Netherlands

Corresponding Publication: ' Electrolyte effects on recirculating dense bubbly flow: An experimental study using X-ray imaging', *AIChE Journal*, DOI: 10.1002/aic.16696

1. Motivation

Airlift bubble column are used in gas-liquid unit operations in industrial chemical and bio-processes: such as waste-water treatment, electrolysis and froth flotations [1]. Presence of dissolved electrolytes (inorganic salts), as surface-active agents, affects an already complex hydrodynamics of bubbly flows, thereby altering the performance of these processes. However, existing design models of these columns are still heavily reliant on data from ideal air-water experiments. A better understanding of electrolyte effects is therefore needed, in order to develop efficient design models for airlift bubble columns.

In current work, hydrodynamics of an internal circulating airlift bubble column, in presence of wide range of electrolyte concentrations (up to 2M NaCl dissolved in water), has been studied. Our results strongly indicate that the role of electrolyte is primarily through the coalescence inhibition and resultant impact on the bubble size distribution (BSD) at fine-pore spargers. The current conclusion is based on measurement of three hydrodynamic parameters:

- Bubble size distribution – measured with high speed imaging
- Local and global gas fraction - measured with X-ray imaging
- Bubble velocity – measured with Bubble imaging Velocimetry (BIV)

In the current effort, all corresponding processed experimental data is provided. The entire set of data can be used to validate CFD models for dense bubbly flows, for which does not exist much detailed data. Further in this document, the experimental setup and the measurement techniques have been explained in detail.

2. Experimental Setup

Experiments are performed in a rectangular internal loop airlift bubble column (W x D x H = 300 mm x 100 mm x 1000 mm), with riser section dimensions equal to W_R x D_R x H_R = 100 mm x 100mm x 400 mm. Schematic of the column is shown in Figure 1.

---

* Corresponding Author: Email: L.portela@tudelft.nl

Spargers: The column is equipped with two ceramic fine-pore diffusers (Pentaires), Ws x Ds x Hs = 25 mm x 75 mm x 25 mm; placed at the bottom of the riser section (200 mm above the bottom of the column). The average pore size of the diffuser is 50µm. The spargers are connected to front end of the column using a sparger plate, that extends 50mm into the riser section. Note: for current purposes the term electrolyte and salt is interchangeably used.

Experimental cases:

- Electrolyte concentrations (moles/L, NaCl): 0, 0.2, 0.5, 1.0, 2.0 M
- Gas superficial velocity, v_{sg} (cm/s): 0.8, 1.6, 3.2, 4.8 (defined as the ratio of the inlet gas flow rate and the c/s area of the riser)

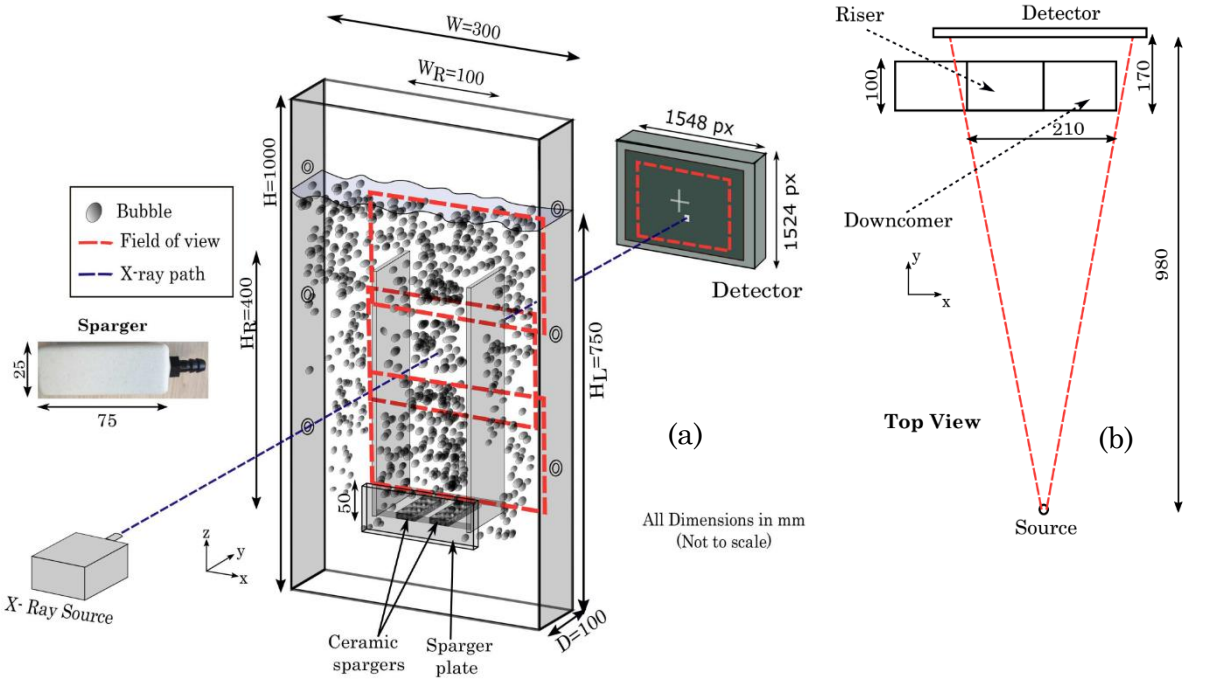

Figure 1: Airlift column setup (a) Schematic with column and sparger dimensions, red dashed lines showing the overlapping X-ray field of views (b) top view showing the location of the column w.r.t. the X-ray source and detector

3. Experimental methods and data

3.1. Flow Profile

Figure 2 shows the effect of electrolyte addition on flow profile in the airlift column. In water case, little to no recirculation of bubbles is observed. Due to a typical low slip velocity, bubbles are dragged into the top part of the downcomer section (below the airlift separator), along with the recirculating liquid. The bubbles are balanced by counteracting buoyancy force, forming a recirculating zone (as schematized in Figure 2a (right)). At higher superficial velocity, a higher gas carryover into the downcomer section is observed, which can be

attributed to an increase in the liquid circulation velocity. Liquid recirculation affects the bubble plume rising from the sparger, meandering the plume towards the center of the riser.

In salt case, smaller bubbles are formed; due to a lack of buoyancy force, these bubbles recirculate into to the downcomer. The recirculating bubbles rise along the walls of the riser section and interact with the bubble plumes above the sparger plate (Figure 3 (right)). There is also a finite foam layer formed at the top surface, as these smaller bubbles do not coalesce to

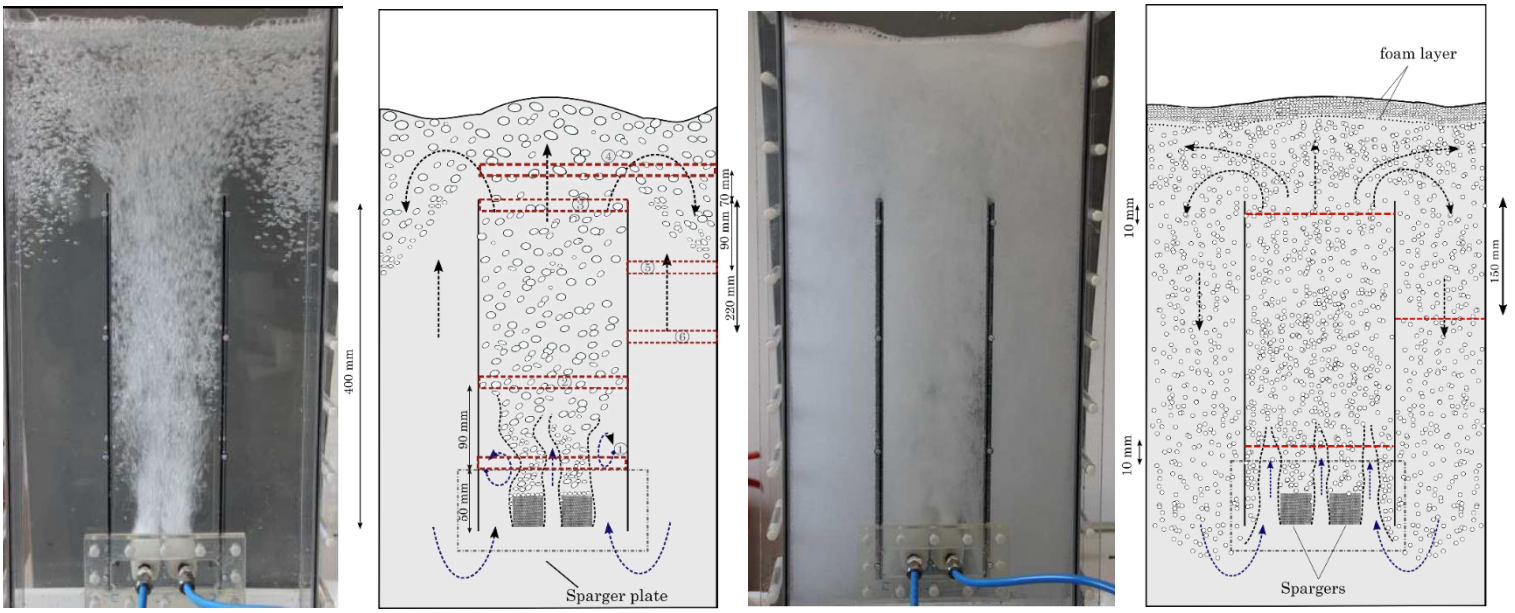

(b) Water case (a) Salt case

Figure 2: Flow profile: (a) Water case; red squares represent the locations of gas fraction measurements and (b) salt cases, (b) Salt case; Red lines represent locations of the bubble size measurements. (left) snapshot of the flow and (right) schematic

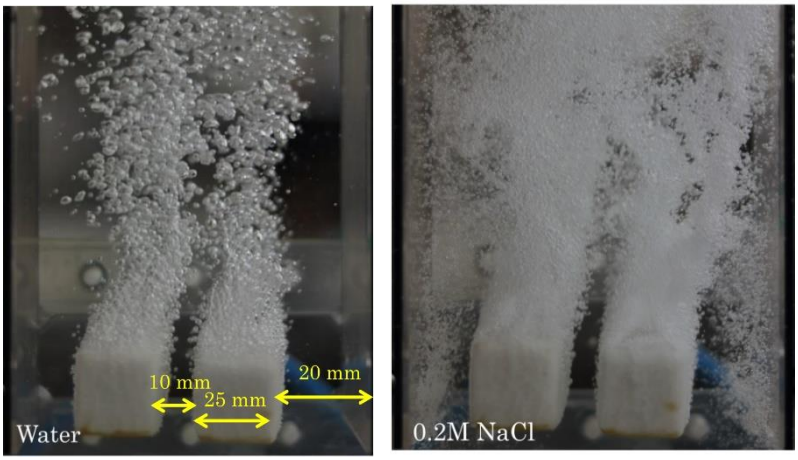

Figure 3: Snapshots of the sparger region (imaged from rear of the column) at v_{sg}=1.6cm/s

Data: Flow profiles are captured as videos using a high-speed digital camera (Canon EOS R with a 50 mm lens) at 100 frames/s at a resolution of 22.3 pixel/mm. Videos are added to the folder *flow-profile*.

3.2. Gas fraction measurements

Purpose: To quantify (i) effect of bubble recirculation on overall gas fraction (ii) effect of the bubble size reduction on bubble plume dynamics.

Method: Gas fraction measurements are performed with X-ray imaging of three overlapping field of views, as shown in Figure 1. Due to presence of the sparger plate, gas fraction measurements are done above the region (position 1 in Figure 2a (right)).

1. Local Gas fraction: Pixel-wise gas fraction, averaged along the X-ray path, is obtained by measuring the intensities with and without the gas bubbles, I_{gas} and I_{nogas} are respectively,

$$\alpha_{g,pixel} = \left(\frac{X_{nogas} - X_{gas}}{X_{nogas}}\right) = \frac{1}{(\mu \cdot X_{nogas})} \cdot \log\left(\frac{I_{gas}}{I_{nogas}}\right)$$

where, μ is the X-ray attenuation coefficient, measured for each pixel by a calibration method.

In order calculate the local gas fraction, the pixel wise data is averaged over a window size of 15mm x 4mm, over a period of 15 seconds (acquisition at 20Hz). This is done in order to reduce the error induced by the blurring motion of the bubbles. Calibration and validation of the gas fraction measurement is explained further in the full-paper.

Lateral gas fraction profiles above the sparger plate, in the riser section, show a M-shaped profile, with the peak corresponding to the positions above the two spargers. With increasing superficial velocity (v_{sg}), there is an increase in overall number of bubbles, and thus an increased gas fraction. However, the lateral profiles are similar in structure (Figure 4 (left)). At a constant flow, with addition of salt, the bubble plume widens; this is a result of the interaction of the bubble plumes with the recirculating bubbles, causing asymmetry in the plume (Figure 4 (right)).

2. Overall gas fraction: Top surface is tracked from the X-ray images using a threshold in the pixel-wise intensity. Increase in the surface height, due to gas addition is used to calculate overall fraction. Note: this height doesn't include the foam layer at the top, as the amount of liquid in the foam is beyond the sensitivity of. Considering that the thickness of the foam is few millimeters, its exclusion introduces an error in the overall gas fraction smaller than 0.4% ($4x10^{-3}$) in absolute value.

Data: Lateral gas faction profile are provided for 6 locations in the airlift column, as shown in Figure 2a (right). These locations are chosen in order to clearly show the effects of the salt concentration and the superficial velocity on the gas recirculation. Overall gas fraction is provided in a separate file for all experimental cases.

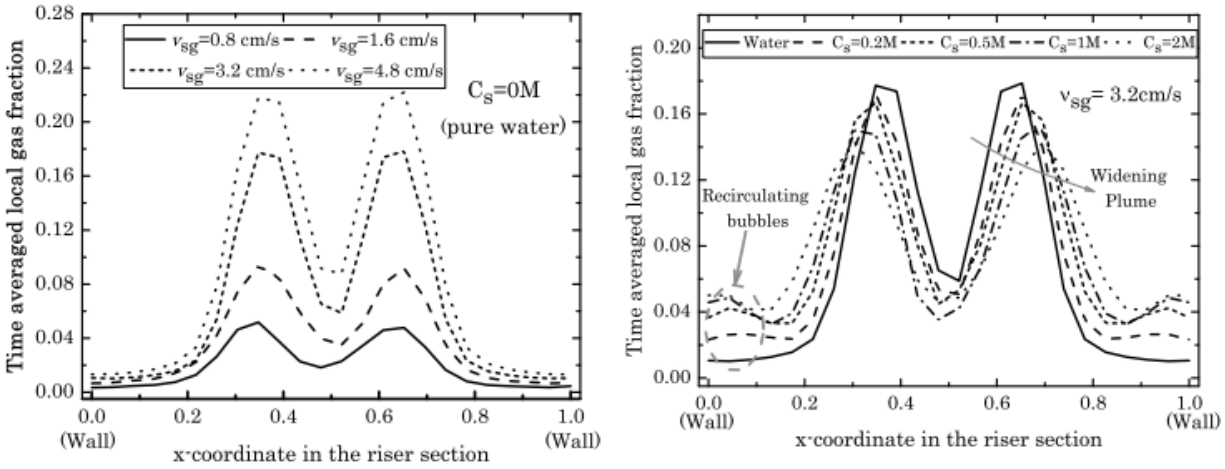

Figure 4 : Gas fraction above the sparger plate (a) effect of superficial velocity without salt (b) effect of salt addition at superficial velocity v_{sg}= 3.2cm/s

3.3. Bubble size measurements

As the direct effect of electrolyte addition is on the bubble size, it is quite important to measure the bubble size distribution. Two different types of bubble size distribution (BSD) measurements have been performed:

1. Individual sparger:
   Purpose: (i) Characterization of fine-pore sparger. (ii) the average of bubble size (figure 5c) is used as an input parameter for an 1D-drift flux model (explained in detail in the full paper).
   Method: Images are captured ~ 10mm above the surface of an individual sparger (mid-depth) placed in a rectangular tank of 250mm (W) x 250mm (H) x120mm(D). Field of view of images is 17mm x 17mm, with pixel resolution is 117.2 pixel/mm . Multiple overlapping field of views are used to obtain the profile along the lateral direction of the plume.
2. Airlift column:
   Purpose: To analyze the effect of recirculation of sub-millimeter bubbles on BSD.
   Method: BSD in riser and downcomer section is obtained in the mid-depth plane and a field of view of images is 17mm x 17mm. As the average bubble size is smaller in the downcomer section, the field of view is reduced to 12mm x 12mm, with a pixel resolution of 168 pixel/mm.

For both purposes, bubble images are captured using a high-speed camera (PCO.dimax s4, 2016 x 2016 pixels) with 75mm lens at an aperture f/1.8. Images are analyzed using open-source image processing software FIJI, to obtain bubble size distribution (BSD). To avoid oversampling of the same bubble, the frame rate is chosen based average velocity of bubble. The processing involves: background subtraction, segmentation of overlapping bubbles (in Matlab), binarization and particle analysis. Shape of each bubble is assumed as an oblate spheroid, with the third coordinate being same as the major axis of the ellipse (obtained from image processing). Bubble diameter is equivalent diameter of a sphere with same volume.

Bubble size distribution is based on a sample size of over 800 bubbles. A large sample is chosen to avoid a bias towards smaller bubbles [2].

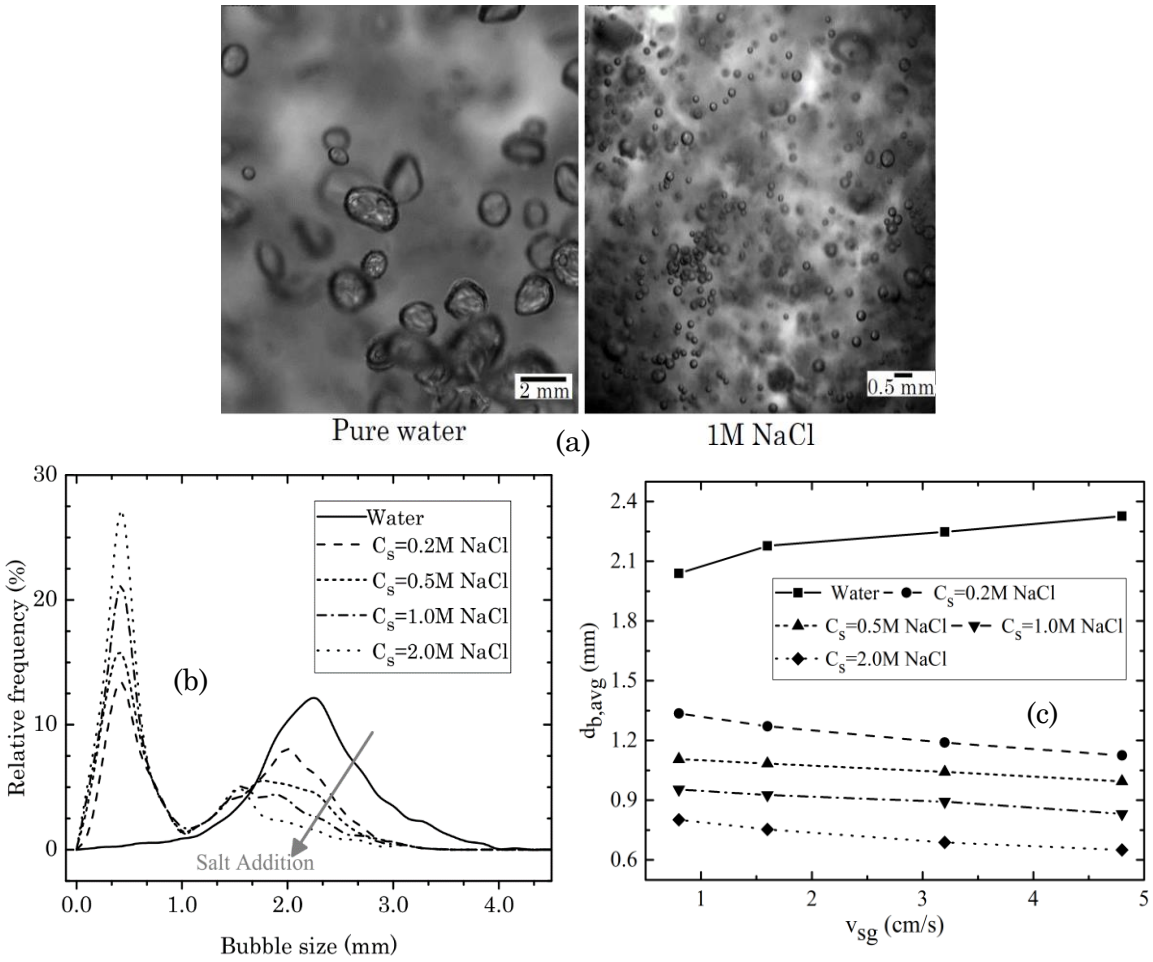

Figure 5: (a) Snapshots of bubble size distribution above the sparger with(out) salt addition. (b) bubble size distribution (BSD) at $v_{sg} = 1.6cm/s$ (c) Effect of gas superficial velocity on average bubble size

With electrolyte addition, typical bubble sizes from an individual sparger reduces from typical ~2 - 3 mm to ~ 200 μm (figure 5a), making the bubble size distribution bimodal. This is a direct consequence of the salt induced coalescence inhibition at the surface of the sparger. With increasing salt concentration and a higher inhibition, fraction of smaller bubbles increases (figure 5b).

3.4. Bubble velocity

Gas-liquid flows in the disengagement section (region between top of riser-downcomer sections and the free surface) is essential in understanding gas carryover into the downcomer. Larger bubbles in this region are driven to the top surface due to buoyancy and smaller ones recirculate into the downcomer.

Purpose: To understand the role of (i) electrolyte induced bubble size distribution on flow recirculation. (ii) dynamics of foam layer.

Method: Bubble imaging velocimetry (BIV) is similar to a traditional PIV technique, however a instead of suspended particles, the motion of bubble interface is tracked, giving a *mosaic* of the gas-liquid motion. Another key difference is the use of a backlight illumination with a shallow focal depth imaging (f/1.8), instead of a laser sheet illumination. Images of the disengagement zone (field of view 20 cm x 20 cm) are acquired at 1000fps. These images are further processed in LaVision Davis 8.0 software in two steps (as illustrated in figure 6).

(i) Pre-processing: Background homogenization, time sequence filter, Image inversion, algorithmic masking.
(ii) PIV processing: Multi-pass correlation with shrinking window size.

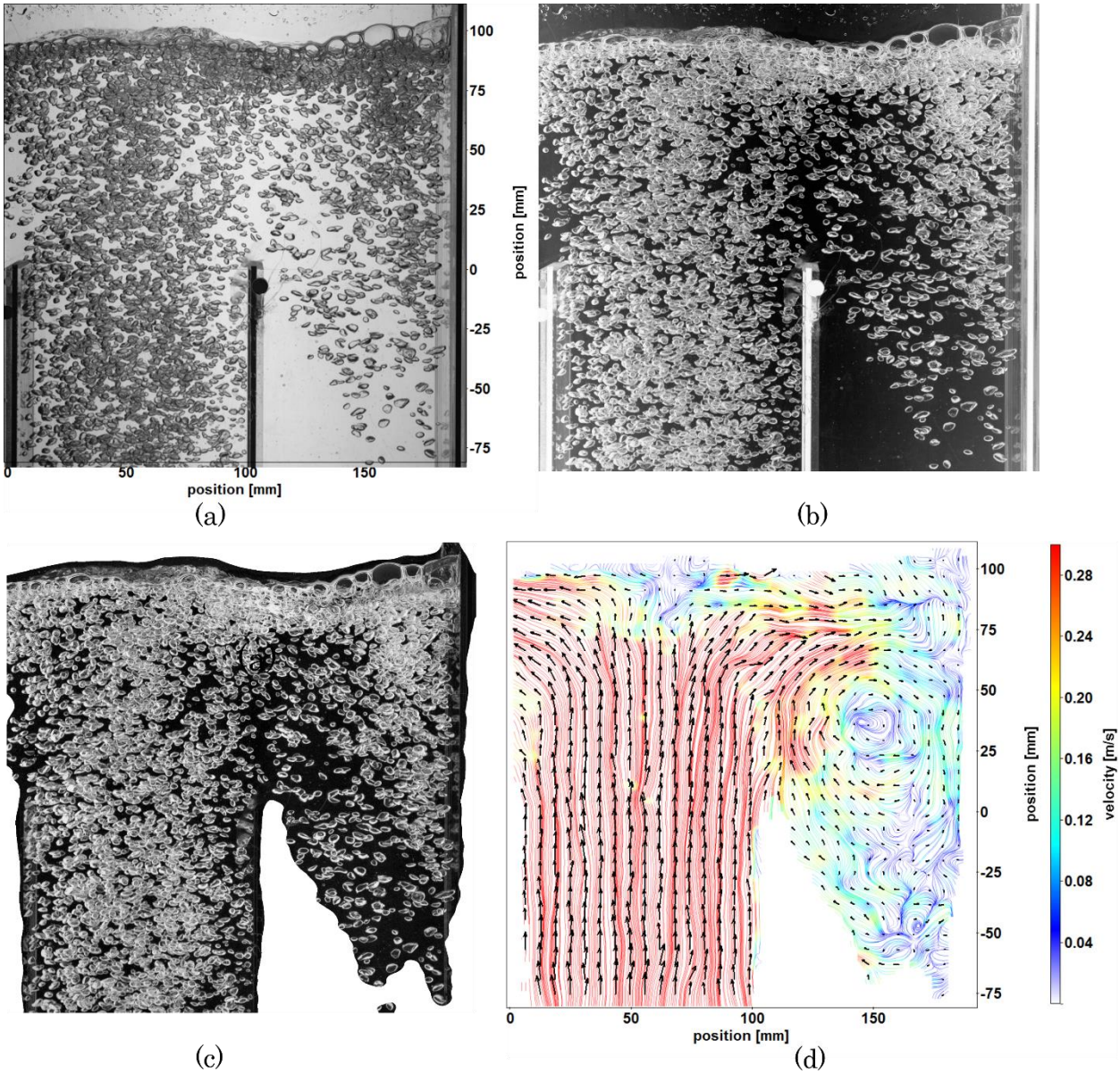

Figure 6: BIV Processing (Water case 10lpm): (a) Raw image (b) Background processing and Inverted image (c) Algorithmic masking to detect bubble-areas (d) after PIV processing

Data: Experiments are performed with water and 0.2M NaCl cases at v_{sg} = 1.6 and 3.2 cm/s to illustrate the effects of salt addition and superficial velocity. Raw images, processed velocity vector data (.vec) files and .xml files (contains PIV processing steps) for all four cases are added in the folder *bubble velocity*. Vector files can be accessed using PIVMat, an open-source Matlab based post-processing toolbox. A detailed stepwise guide has been added as well.

This work is part of the Industrial Partnership Programme i36 Dense Bubbly Flows, that is carried out under an agreement between Nouryon Industrial Chemicals B.V., DSM Innovation Center B.V., SABIC Global Technologies B.V., Shell Global Solutions B.V., Tata Steel Nederland Technology B.V. and the Netherlands Organization for Scientific Research (NWO).

4. References

[1] N. Deen, R. Mudde, J. Kuipers, P. Zehner, and M. Kraume, "Bubble Columns," *Ullmann's Encyclopedia of Industrial Chemistry*, Wiley-VCH Verlag GmbH & Co., 2010.

[2] G. Besagni, P. Brazzale, A. Fiocca, and F. Inzoli, "Estimation of bubble size distributions and shapes in two-phase bubble column using image analysis and optical probes," *Flow Measurement and Instrumentation*, vol. 52, 2016, pp. 190–207.